HHS Public Access

Author manuscript

Nat Med. Author manuscript; available in PMC 2020 October 07.

Published in final edited form as:

Nat Med. 2019 October ; 25(10): 1512–1518. doi:10.1038/s41591-019-0598-9.

A luminal unfolding microneedle injector for oral delivery of macromolecules

Alex Abramson[1,$], **Ester Caffarel-Salvador**[1,2,$], **Vance Soares**[1], **Daniel Minahan**[1], **Ryan Yu Tian**[1], **Xiaoya Lu**[1], **David Dellal**[3], **Yuan Gao**[1], **Soyoung Kim**[1], **Jacob Wainer**[1], **Joy Collins**[1], **Siddartha Tamang**[1], **Alison Hayward**[1,5], **Tadayuki Yoshitake**[8], **Hsiang-Chieh Lee**[8], **James Fujimoto**[8], **Johannes Fels**[4], **Morten Revsgaard Frederiksen**[4], **Ulrik Rahbek**[4], **Niclas Roxhed**[1,6], **Robert Langer**[1,2,7,*], **Giovanni Traverso**[1,3,9,*]

[1]Department of Chemical Engineering and David H. Koch Institute for Integrative Cancer Research, Massachusetts Institute of Technology, Cambridge, MA 02139

[2]Institute for Medical Engineering and Science, Massachusetts Institute of Technology, Cambridge, MA 02139

[3]Department of Mechanical Engineering, Massachusetts Institute of Technology, Cambridge, MA 02139

[4]Global Research Technologies, Global Drug Discovery, and Device R&D, Novo Nordisk A/S, Maaloev, Denmark

[5]Division of Comparative Medicine, Massachusetts Institute of Technology, Cambridge, MA 02139

[6]Department of Micro and Nanosystems, KTH Royal Institute of Technology, Stockholm, Sweden

[7]Media Lab, Massachusetts Institute of Technology, Cambridge, MA 02139

[8]Department of Electrical Engineering and Computer Science and Research Laboratory of Electronics, Massachusetts Institute of Technology, Cambridge, MA 02139

[9]Division of Gastroenterology, Brigham and Women's Hospital, Harvard Medical School, Boston, MA 02115

Abstract

Insulin and other injectable biologic drugs have transformed the treatment of patients suffering from diabetes. Patients and healthcare providers, however, prefer the oral route of administration, yet macromolecule drugs are not readily absorbed into the bloodstream through the gastrointestinal tract. We developed an ingestible capsule, termed the luminal unfolding

*Correspondence to: ctraverso@bwh.harvard.edu, cgt20@mit.edu; rlanger@mit.edu.

$Authors contributed equally

Contributions: A.A., E.C-S., designed the study, performed experiments, analyzed and interpreted data, and wrote the manuscript. V.S., D.M., X.L., R.Y.T., D.D., Y.G., S.K., J.W., J.F., M.R.F., N.R., designed, fabricated and evaluated prototypes of the system. J.C., S.T., A.H., designed, performed and helped analyze in vivo evaluation of the system. T.Y., H-C. L., J.F., designed, performed and interpreted characterization of prototype tissue interactions, U.R., R.L., G.T., designed, supervised, reviewed the data and edited the manuscript.

Competing Interests: A.A., E.C-S., D.D., N.R., M.R.F., Y.G., R.L. and G.T. are co-inventors on multiple patent applications describing oral biologic drug delivery. J.F., M.R.F. and U.R. work for Novo Nordisk. R.L. and G.T. report receiving consulting fees from Novo Nordisk.

microneedle injector (LUMI), which allows for the oral delivery of biologic drugs by rapidly propelling dissolvable drug-loaded microneedles into intestinal tissue using a set of unfolding arms. During ex vivo human and in vivo swine studies the device functioned safely and efficaciously. Using insulin as a model drug, we showed that after actuation the LUMI provided a faster pharmacokinetic uptake profile and a systemic uptake greater than 10% compared to subcutaneous injection over a 4 hour sampling period. With the ability to load a multitude of microneedle formulations, the device can serve as a platform technology to orally deliver therapeutic doses of macromolecule drugs.

Introduction

Patients prefer oral formulations over injections[1], and this affects how they choose to treat life-threatening illnesses such as diabetes[2]. Public health experts have surveyed patients suffering from diabetes, and these studies have demonstrated that adding the burden of daily or weekly dosing regimens requiring injections creates the same order of magnitude of patient disutility as the disease itself[3]. Compared to subcutaneously administered biomacromolecule drugs, oral formulations of active pharmaceutical ingredients (APIs) create less patient discomfort[4], demonstrate greater stability in high temperature environments[5], and don't generate biohazardous needle waste[6]; however, capsule based small molecule pharmaceuticals generally provide inferior health outcomes compared to biologic drugs requiring injection[7,8]. Nevertheless, healthcare providers often prescribe injectable drugs only after oral agents fail to control the disease[9–11]. Physicians and patients delay insulin initiation an average of 7.7 years after initiation is clinically recommended [9,11]. Since insulin was first injected into a human subject in 1922, scientists have explored methods to orally formulate biologic macromolecules and make them easier for patients to take[12]. Specifically, they have focused on delivering these drugs through the small intestine. While we have previously demonstrated the ability to deliver macromolecule drugs via a capsule-based injection to the stomach[5], the small intestine's extensive surface area and vascular system provides the potential for enhanced uptake into the bloodstream compared to the subcutaneous space and other areas of the gastrointestinal (GI) tract[13,14]. In order to achieve systemic bioavailability, orally delivered biomacromolecules must navigate through biological systems in the GI tract designed to prevent undigested protein absorbsion[15–17].

Diffusion across the mucus and tissue layers of the GI tract fundamentally limits oral bioavailability[18]. Researchers have developed permeation enhancers[19,20], nanoparticle encapsulations[21,22] and mucus adhering patches[23,24] to enhance drug uptake. These innovations, however, dampen pharmacokinetics[20,24] and reduce bioavailability[25] compared to dosing via parenteral routes due to enzymatic degradation and slow uptake. To address these problems, we created an orally dosed device which physically inserts drug loaded microneedles into the small intestine and bypasses the need for diffusion into the tissue wall. The device holds a clinically relevant drug load, provides faster systemic uptake after actuation compared to subcutaneous injection, and provides a systemic bioavailability greater than 10% that of a subcutaneous injection over a 4 hour sampling period.

While several safety concerns surround the process of injection in the GI tract, retrospective analyses demonstrate this action's safety. Gastroenterologists regularly employ a 5 mm long 25 gauge needle to inject saline into the small intestine and colon wall with complication rates lower than 1 in 1000[26,27]. Additionally, case studies on swallowed sharp objects such as razor blades and needles demonstrate that the small intestine safely withstands transiting sharp objects up to 1 cm in length[14,28,29]. Also, the GI tissue regenerates quickly, ensuring that any injection damage rapidly repairs itself[30,31].

In order to design a safe enteric microneedle capsule, we performed multiple mechanical characterization studies in the small intestine. Here we report an evaluation of needle penetration in ex vivo human and in vivo swine small intestine that denotes force and displacement values associated with tissue perforation. Using this data we developed a safe, orally dosed luminal unfolding microneedle injector (LUMI) with the potential to replace subcutaneous macromolecule injections (Figure 1, 2a). The device, which rapidly unfolds in the small intestine to insert microneedles into the tissue, acts as a platform technology and provides the ability to load different microneedle formulations with various APIs. As a proof of concept to support the capacity of the device to deliver a macromolecules across the GI tract to achieve systemic bioavailability, we used a microneedle patch which delivered biologically relevant doses of insulin with concomitant hypoglycemia in an in vivo swine model.

Results

Engineering the Device

The LUMI device utilized the tube-like geometry of the small intestine to create multiple points of contact with the tissue (Figure 2a-e). Initially delivered in a custom designed enteric capsule, the device employed an elastomeric core to quickly unfold and expand within the GI tract. Each of the device's three degradable arms propelled a dissolving drug loaded microneedle patch into the tissue wall. These arms stretched the tissue in multiple directions and allowed the tissue to exert an opposing force on the microneedles. We optimized the force from the elastomer to ensure microneedle penetration while avoiding perforation. The elastomeric core and the arm geometry maximized both the safety and efficacy of the system.

When exiting the capsule, the LUMI can open in any orientation relative to the small intestine. We specifically studied the deployment from two orientations: axially symmetric or parallel to the central axis of the small intestine (Figure 2b). These two orientations were the alignments at which the LUMI provided the greatest and least amount of tissue stretching, respectively. A geometric analysis of the opening event (Supplementary Information) allowed us to design the LUMI with an arm length long enough to ensure that the microneedles always made contact with and stretched the tissue wall regardless of the LUMI's orientation within the small intestine. Figure 3c demonstrates the ability for the tissue, when stretched, to conform around the microneedle patch.

In order to ensure that the LUMI arms exerted enough force on the tissue for microneedle insertion, we optimized the device's arm length and the core strength (Figure 2f-k, S1,

Supplementary Text). We incorporated a spring steel component into the central unfolding elastomer to increase the unfolding force and prevent the arms from twisting or deflecting away from the tissue during actuation. Devices were optimized via in vivo experiments to orient most frequently in the axial direction to provide the greatest amount of force for microneedle insertion.

In order to deliver the LUMI device to the small intestine while preventing dissolution of the microneedles prior to insertion, we designed a custom capsule that allowed the device to remain separated from fluid until seconds before actuation. The capsule measured 9 mm in diameter and 30 mm in length (Figure 2e). Importantly, the capsule possessed two chambers. One section was waterproof and contained the LUMI device while the other one possessed a moisture and pH activated actuation mechanism made from a polyethylene glycol (PEG) encapsulated compressed spring and a pH sensitive Poly[methacylic acid-co-ethyl acrylate] coating. This coating was tuned to dissolve at a pH of 5.5 or greater, a value experienced in the duodenum but not in the stomach[32]. The efficacy of the pH sensitive coating was verified in vitro by placing the capsules in buffers of increasing pH starting at pH 2. Figure 2a describes the timeline of capsule deployment after entering the small intestine, and a written explanation is found in the supplementary text. X-ray imaging confirmed that capsule actuation occurred within two hours of residing in the small intestine in vivo (Figure 2c). In vitro, we demonstrated that actuation mechanisms made from different molecular weights of PEG allowed the capsule to actuate over different time scales from 1.5–5 hours after entering an environment with a pH of greater than 5.5 (Figure 2l).

We designed the LUMI device's unfolding arms so that once the capsule actuated they maintained enough strength to deliver the drug payload in vivo while still dissolving in a timely manner to prevent obstruction. Fabricated from mixtures of biodegradable polyethylene oxide (PEO) and Soluplus® (polyvinyl caprolactam-polyvinyl acetate-polyethylene glycol graft copolymer (PCL-PVAc-PEG)), the arms degraded within 24 hours in vitro and in vivo (Figure S2, S3); however, the arms retained enough mechanical strength 10 minutes into degradation to remain intact and push against the tissue wall as determined via a three-point bend test in vitro (Figure 2m). Spacing between the arms allowed for chyme to pass around the device and mitigate the risk of obstruction while the LUMI was in an unfolded state.

Just as the arms were designed to reduce intestinal obstructions, the capsule was also constructed to mitigate this issue. After the LUMI device was ejected, the same holes used to allow fluid to dissolve the actuation mechanism permitted the passage of intestinal fluid through the capsule. Additionally, we fabricated the capsule so that the walls consisted of multiple pieces no larger than 9 mm in diameter and 15 mm in length (Figure 2e). The wall pieces were held together via a pH sensitive polymer coating which dissolved at pH 7.0 or greater, a value felt in the lower intestine but not in the upper portion of the small intestine[32]. We demonstrated in vitro that the coating kept the capsule intact during device actuation, yet within two hours after entering an environment with a pH greater than 7, the capsule broke into multiple pieces. We verified that coated capsules delivered in vivo to swine lost mechanical integrity at this junction point by retrieving and inspecting them post excretion.

The non-degradable elastomeric core of the LUMI, measuring 12 mm in diameter and 1.5 mm in height, passed through the GI tract along with the capsule parts without issue during all in vivo experiments. In one experiment, we fed a total of 12 capsules and 12 LUMI devices to the stomachs of three different swine. Radiographs confirmed the passage and excretion of all devices, and at least one device was retrieved intact and examined after excretion from each swine. The 8 devices not retrieved were lost in the cage bedding. We performed upper and lower endoscopies on the animals after the devices were excreted, and we saw no abnormalities caused by the devices in the stomach, small intestine, colon, or rectum. After euthanasia, the GI tracts of all of the animals were examined; no gross abnormalities caused by the devices were observed, and no devices remained inside of the body.

Engineering the Microneedles

We performed penetration experiments on ex vivo human small intestine tissue as well as on ex vivo and in vivo swine tissue to determine the force and distance required for penetration while avoiding a full thickness perforation (Figure 3g-h, S4). Force measurements showed that needles entered the tissue after applying as low as 5 mN of force. The needles reached a displacement of over 6 mm before perforating the outermost tissue layer. Perforation forces for a single needle into in vivo swine tissue ranged from 0.27 N – 0.53 N, compared to 0.20 N - 0.28 N for ex vivo human tissue perforation. This suggests that the issue of perforation could be managed by limiting the applied force and the length of the needles used in the LUMI.

Using these results, we designed a system which delivered patches containing 32 microneedles on each arm measuring 1 mm in height. The simultaneous delivery of multiple microneedles dispersed the applied force over all microneedles (“bed of needles” effect), and the microneedle height limited the ability for the device to perforate the tissue. In order to ensure penetration, the LUMI arms applied a contact force measuring 0.41 ± 0.06 N, or 13 mN per microneedle. Multiple imaging techniques confirmed microneedle penetration in ex vivo small intestine tissue. MicroCT pictures of LUMI devices loaded with barium sulfate microneedle patches (Figure 3c) and hypodermic needles (Figure S5) demonstrated tissue penetration in ex vivo small intestine without perforation as denoted by the pink dotted lines. These results were further supported using histology where hypodermic needles coated with tissue marking dye penetrated 800 μm through the tissue when deployed using the LUMI (Figure 3e). The absence of dye in the 1 mm thick slice suggested that the needle did not reach this depth, reassuring its inability of perforating the small intestine. Optical coherence tomography (OCT) also confirmed microneedle penetration after the manual insertion of a patch (Figure 3i) or deployment of a single LUMI arm into the tissue from a 30 degree angle (Figure S6). To demonstrate microneedle penetration in vivo and assess the effects of needle insertion on live tissue, histology was taken after dosing to sedated swine (Figure 4). As a control, microneedle insertion was compared to insertion of a 32 G needle coated in blue tissue marking dye. Using the data collected which assessed tissue engagement, we developed a microneedle patch platform for the LUMI to deliver high loads of API.

The drug load on the LUMI was limited by a variety of factors, including: drug loading fraction; microneedle width and height; and microneedle density on the patch. We developed a method for microneedle fabrication utilizing API powder in order to increase the drug loading for the LUMI device (Figure 3a). The microneedle patch was incorporated into the LUMI arm in an outward configuration (Figure 3b) with an indentation in the arm in order to prevent needle breakage during encapsulation. The microneedles were spaced only 800 μm apart from tip to tip to ensure a high needle density on the patch. Each LUMI device held one microneedle patch on each arm, and the entire device possessed a total microneedle footprint area of 0.5 cm^2. This allowed the LUMI to hold up to 0.3 mg of drug. We demonstrated the ability for the LUMI to load multiple formulations and active pharmaceutical ingredients by incorporating microneedle patches made with insulin, lysozyme and alpha-glucosidase onto the LUMI (Figure S7–8). These included patches which used either polyvinylpyrrolidone or sorbitol as a binding ingredient. Microneedle dissolution and drug deliver kinetics were studied in vitro (Supplementary text and Figures 3d, 3f, 3i, S9-S13) prior to in vivo evaluation.

In vivo Pharmacokinetics Experiments

When LUMI devices were deployed in vivo in the swine small intestine a peak plasma insulin concentration was observed approximately 25 minutes after actuation with associated hypoglycemia. During each set of swine trials, a 1 cm^2 microneedle patch was loaded with 0.6 mg of insulin and delivered in one of four ways (n=3 for each approach): the patch was applied directly to the small intestine tissue; the patch was cut into pieces and loaded onto two LUMI devices for deployment in the jejunum; the needles on the patch were dissolved in 0.5 mL of sterile saline, filtered through a low protein binding sterilization filter, and administered subcutaneously; or the needles were dissolved in 10 mL of water and administered into the lumen of the jejunum via an endoscope. During filtration for the subcutaneous dosing some of the insulin was lost in the filter, and the final calculated insulin dose was 0.2 mg. Blood glucose level changes were recorded over 4 hours and dextrose was administered when hypoglycemia was observed. The LUMI method of delivery provided a 44% ± 5% blood glucose drop over 60 minutes, and all LUMI trials showed insulin uptake and a blood glucose drop (Figure 5a). Comparably, subcutaneous injection and small intestine patch application produced similar blood glucose drops with a 64% ± 12% and 54% ± 8%, respectively. However, when the solution with solubilized microneedles was administered into the jejunal lumen, it yielded no significant blood glucose level changes (Figure 5a).

A pharmacokinetic comparison across different administration methods of microneedles loaded with insulin is shown in Figure 5b. These experiments demonstrated that swine dosed with microneedles applied to the small intestine via the LUMI or via a manually applied patch reached their peak plasma concentrations at 25 minutes (t_{max}). Comparably, those dosed with a subcutaneously injected solution of dissolved microneedles experienced a t_{max} at 90 minutes. This result illustrates a more rapid onset of insulin action achieved by microneedle injection to the small intestine compared to subcutaneous dosing. The LUMI dosing and subcutaneous administration showed similar peak plasma levels (C_{max}) of 46 ± 15 pM and 39 ± 15 pM, respectively (Figure 5b). Over the 4 hour sampling period, the

microneedle patch directly applied to the small intestine dosing 0.6 mg of insulin and the subcutaneously dosed 0.2 mg of insulin showed an equivalent systemic drug uptake. Over the 4 hour sampling period, the insulin delivered by the LUMI showed 40% systemic uptake compared to the directly applied patch and over 10% systemic uptake compared to the subcutaneous injection. Projected out to infinite time, the directly applied microneedle patch systemically delivered 80% of the subcutaneous dose (Figure 5c).

Discussion:

Here we report the development of a system which demonstrated safe and efficacious biologic delivery in the small intestine of a swine model. The tissue penetration tests we performed with human and swine tissue, in combination with the “bed of needles” effect, reinforced the notion that the LUMI provided means to mitigate the potential risk of microneedle perforation. A device containing 30 microneedles would require on the order of 3 N to perforate the tissue with each needle. The LUMI delivered one order of magnitude less force. Still, it was possible that a device would deliver an array of needles such that the force was unevenly distributed. In fact, literature on transdermal microneedle patch delivery demonstrated that applicators applied a disproportionate amount of force to microneedles on the corners of patches[33]. The small intestine in particular possessed an uneven surface due to folds and villi projections, which made the tissue more susceptible to uneven force distributions. Our experiments, supported through histology, OCT, and microCT, showed that no perforation event occurred during any LUMI deployment. This included a deployment where a LUMI containing a single hypodermic needle on each arm was actuated in small intestine tissue. Another factor to consider is the age of the patient receiving the device, as the risk of bowel perforation is known to increase with age[34]. To address this issue, we performed our needle penetration characterization studies on human tissue samples from patients aged 32, 45, and 70 and used the information from all three samples to determine LUMI device design specifications. While further tests will be necessary during translation, the LUMI’s design significantly mitigates perforation risk.

The risk of small intestine obstruction, a medical condition sometimes requiring hospitalization and surgery, increases with the presence of large non-degradable objects in the GI lumen. We designed the LUMI device to dissolve and break apart into small pieces to avoid this complication. The LUMI utilized the OROS osmotic pump capsule, a daily dosed and non-degrading drug delivery device, as a model to guide device and individual component size. One version of the OROS measured 12 mm in diameter and 5 mm in thickness with an obstruction rate of less than 1 in 50 million during commercialization[35]. Another version of the OROS measured 9 mm in diameter and 15 mm in length with a GI retention rate of only 1 in 22 million[35]. During deployment and before degradation, the LUMI reached a size greater than the OROS capsule; however, paths for chyme to travel between the arms of the device mitigated the risk of obstruction. After the LUMI arms dissolved, only the non-degradable LUMI core remained. This core measured 1.5 mm thick and 12 mm in diameter, smaller than the OROS system. The metal component in the core remained fully encapsulated inside the elastomer during degradation and did not make contact with the tissue. The non-degradable LUMI capsule contained holes after actuation which allowed chyme to pass through and also possessed the ability to break up into pieces 9

mm in diameter and 15 mm in length (comparable in size to the second OROS system) after entering the lower intestine. Therefore, we expect that the rates of gastric obstruction would remain comparable to the OROS solid dosage forms.[35]. After exiting the body non-degradable solid dosage forms approved by the FDA, such as the OROS system, are removed from the waste stream by the sewage treatment facilities[35,36]. Because the LUMI possesses a similar size and material make-up to these FDA approved capsules, we anticipate that LUMI would have a comparable FDA environmental assessment.

Of note, the LUMI's metal components could interfere with MRI machines. Hence, patients would need to disclose the intake of the pill during such procedures. Furthermore, future versions of the system could be fabricated of other materials, including polymeric springs to minimize potential interactions with imaging modalities.

While certain sensations such as pain from injection do not usually manifest in the GI tract, discomfort arises when the small intestine is distended[37,38]. Because the LUMI device functioned by stretching the small intestine to inject needles, discomfort may have arisen during device actuation. This will be an important aspect to delineate in early clinical evaluation of systems which expand in the GI tract. In our studies we monitored the swine daily after delivering the devices, and they showed no signs of discomfort (e.g. change in feeding habit, abnormal behavior in socializing and within the disclosure). The fast dissolution time for the arms ensured that the stretch would only occur for as long as necessary to deliver the drug payload. No changes in behavior or appetite were noted during capsule excretion. During future studies in awake animals, we plan to monitor the severity and length of negative sensations, if any, due to LUMI expansion. Additionally, future long term studies will be required to understand the effects of chronic injections into the mucosa of the small intestine; however, during our studies we did not observe any signs of inflammation immediately after delivering the device, moreover histology from the sites of injection showed that the intestinal mucosa showed minimal damage after device deployment. Furthermore, given the length of the small intestine, the LUMI may not target the same area of tissue during every deployment.

Importantly, the LUMI device relied on gastric emptying to move from the stomach to the small intestine. Gastric emptying times can vary significantly in the population. Emptying typically occurs in 1–4 hours, but individuals experiencing gastroparesis - common in diabetic patients - may face gastric emptying times as long as 24 hours[39,40]. This variability leads to an uncertainty in onset of drug action which limits the LUMI to APIs that are not time specific. Such a limitation exists for all enteric capsules and devices. Most of the literature on oral macromolecule drug delivery utilizes enteric capsules, and this presents an important aspect that will require further investigation for the field. For these same reasons, we were unable to deliver the LUMI device to the stomach during our in vivo trials measuring drug pharmacokinetics; however, the coating on the capsule protecting the LUMI from deploying in the stomach was demonstrated to work in vitro and has been shown in other human and animal studies to dissolve only in the small intestine and not in the stomach[20,41]. We also demonstrated in vivo the ability for capsules to pass from the stomach to the small intestine. Our pharmacokinetics studies demonstrated that hypoglycemic onset for insulin delivered via the small intestine occurred more quickly than subcutaneous dosing,

but this did not factor into account the time necessary for the device to reach the duodenum. We also showed that our capsule could release the LUMI after spending different amounts of time in the small intestine, potentially allowing us to tune the delivery time for patients with delayed or enhanced peristalsis. Nevertheless, the post-administration hypoglycemic onset time may be delayed by several hours as the device travels the small intestine.

Ultimately, the LUMI device demonstrated safe and effective deployment into the small intestinal mucosa during preclinical in vivo swine studies. While recombinant human insulin was used as a model drug in the study, the LUMI may not provide the optimal method of drug delivery for this API due to the delayed drug release caused by slow gastric emptying. A drug with an extended half-life such as long acting insulin may be better suited to be delivered by the LUMI because of the potential variability in dosing time caused by digestion. Additionally, the LUMI could potentially load numerous drug formulations mentioned in the microneedle literature. These include vaccines, monoclonal antibodies, enzymes, hormones, RNA, and many other compounds which currently lack oral formulations[42,43]. Macromolecule drugs that are not conducive to subdermal injection due to local skin reactions, such as oligonucleotides[44] and certain TNF-α inhibitors, would be particularly interesting targets to study using this drug delivery method. Compared to delivering drugs into the subcutaneous space, the volume restrictions (and therefore dose restriction), the different enzyme activity levels, protein binding characteristics, and pH in the small intestine tissue may affect the pharmacokinetics and efficacy of some of these drugs delivered via the LUMI system. Further studies exploring a range of APIs are warranted, as clinical translation of orally delivered GI microneedle injections could lead to a paradigm shift in the delivery of macromolecules.

Materials and Methods

Materials

Dulbecco’s Phosphate-Buffered Saline (PBS) was purchased from Gibco by Life Technologies (Woburn, USA). Human insulin was obtained from Novo Nordisk (Maalov, Denmark). Soluplus® (polyvinyl caprolactam-polyvinyl acetate-polyethylene glycol graft copolymer (PCL-PVAc-PEG)) was purchased from BASF (Ludwigshafen, Germany). The 100,000 and 200,000 molecular weight poly(ethylene oxide) (PEO), along with the sulforhodamine 101 acid chloride (Texas red), triethyl citrate, talc, acetone, isopropanol lysozyme from chicken egg, potassium phosphate monobasic solution, potassium phosphate dibasic solution, potassium hydroxide, HCl, *Micrococcus lysodeikitcus* lyophilized cells, bicinchroninic acid kit, α-glucosidase from Saccharomyces cerevisiae, and α-glucosidase activity assay were purchased from Sigma Aldrich (Natick, USA). Polyvinylpyrrolidone, average M.W. 58,000, was obtained from Alfa Aesar (Haverhill, USA). Compressed nitrogen gas was purchased from Airgas (Radnor, USA). Polydimethylsiloxane (PDMS) Sylgard 184 was purchased from Dow Corning (Midland, USA). Female Yorkshire swine were obtained from Tufts University (Grafton, USA) and excised swine tissue from the Blood Farm Slaughterhouse (West Groton, USA). Cadaveric human tissue was provided within 24 h of retrieval by the National Disease Research Interchange (NDRI, Philadelphia, USA). The Blue CDI’s Tissue Marking Dye® was purchased from Cancer Diagnostics

(Durham, USA). Mediprene 4410-LP11L was obtained from Lubrizol (Wickliffe, USA). Eudragit L 100–55 and Eudragit S100 were obtained from Evonik (Essen, Germany). 316 stainless steel shim stock was obtained from McMaster Carr (Elmhurst, USA).

LUMI fabrication

Three dimensional LUMI models were designed in Solidworks (Dassault Systemes, Velizy-Villacoublay, France) and printed out on an Objet 30 Pro 3D printer (Stratasys, Eden Prairie, USA). A negative mold was created out of PDMS (Figure S14). Stainless steel cores milled on an OtherMill V2 (Bantam Tools, Berkeley, CA) were encased in Mediprene and added to the center core of the mold. A mixture of 25% Soluplus® and 75% PEO 200 kDa was microcompounded on an Xplore™ twin screw microcompounder (Xplore™ Instruments, Netherlands) at 50 rpm. This mixture was added to the arm sections of the mold. Using a Master-Mite model 10008 heat gun (McMaster Carr, Elmhurst, IL), the materials were melted in the mold. The metal core was aligned to the center of the device. Pressure was then applied to the mold and the materials were allowed to cool.

Fabricated microneedle patches were then placed on the recessed sections of the LUMI arms. The base plates of the patches were sanded down to a thickness of 1 mm and the patches were cut into 4 × 8 arrays of drug loaded microneedles. The arms of the device were then reheated using a heat gun, and the patches were placed into the melted recessed sections of the arms.

Tissue Perforation Characterization

All animal experiments were approved by and performed in accordance with the Committee on Animal Care at MIT. Single hypodermic needle perforation testing *in vivo* was performed by affixing a needle to a 10 N Shimpo force gauge (Cedarhurst, USA). The force gauge was attached to an arm on a custom stage. We used a motor to move the arm downwards at a rate of 0.2 mm/s. We placed a camera on the moving stage to visualize the penetration event. The force measurements and video feed were recorded in LabVIEW (National Instruments, Austin, USA). In a non-survival experiment, we sedated Yorkshire swine as described in the *in vivo* section, and we performed a laparotomy procedure to access the small intestine. A 5 cm incision was made in the small intestine to reveal a working area of 5 cm by 1.5 cm, and the tissue was fixed so that it was held taut. The needle was then placed directly over the tissue and moved downward at the defined rate until we were able to visualize the needle on the other side of the tissue. All perforation events were correlated to a force drop. Breathing affected intraoperative measurements, and we determined that the displacement caused by the breathing accounted for an extra 3 mm of penetration. We measured this distance change using a ruler and confirmed it by analyzing the force vs displacement curves. We confirmed that forces during the exhaled state were equivalent to forces during the inhaled state 3 mm earlier.

Single hypodermic needle perforation testing *ex vivo* was performed using an Instron 5943 machine equipped with a 10 N load cell (Norwood, USA). Harvested tissue was affixed to a corkboard with a 2.5 cm diameter hole. Needles were fixed to the Instron machine's cross-

head and lowered into the tissue above the hole at a rate of 0.1 mm/s until we visualized the needle on the other side of the tissue. All perforation events were correlated to a force drop.

LUMI arm dissolution characterization

Mixtures of either 100 kDa or 200 kDa PEO and Soluplus® were combined in an Xplore™ twin screw microcompounder (Xplore™ Instruments, Netherlands) at 50 rpm. The extruded material was captured in an Xplore™ 5.5 cm^3 laboratory injection molding machine and molded in to an equilateral triangular prism with side lengths of 3.6 mm and a height of 18.55 mm. The machine exerted 3 bars of pressure for 1 s, ramped up to 4.5 bar over 1 s, and held a pressure of 4.5 bar for an additional 5 s.

Homemade Simulated Intestinal Fluid (SIF) was made by mixing 6.8 g of KH_2PO_4 Potassium phosphate monobasic (Sigma Aldrich) with 0.896 g NaOH (Sigma Aldrich) in 1 L of nanopure water. The pH was confirmed to be at 6.8 using the Mettler Toledo FiveGo pH meter (Columbus, USA).

Eight 250 mL Falcon tissue culture flasks (Corning, Corning, USA) were labeled and used to house each mixture. A volume of 225 mL of SIF was inserted into each flask and stored at 37°C in an Innova 44 incubator (Eppendorf, Hamburg, Germany) which was being shaken at 50 rpm. The 50 rpm agitation simulated the intestinal environment. The flasks containing only SIF were left in the incubator for 6 hours to allow for temperature equilibration. One extruded shape was dropped inside each flask. The shapes were photographed at the 0 h, 1.67 h and 22.5 h time points and the appearance of the arms and the SIF were noted (Fig. S2).

Additionally, the mechanical properties of the PEO and Soluplus® mixtures were determined during the dissolution process. Using the same microcompounding and extrusion method described above, bars of the mixtures measuring 3.2 mm x 12.8 mm x 63.5 mm were created. Three-point bend tests were performed on the bars using a uniaxial mechanical tester (Instron 5943, Norwood, USA). These bend tests were performed on bars that were not placed in any liquid bath as well as bars that were placed in a shaken and incubated mixture of SIF for 10 minutes. Bars were fixed on a three-point bend fixture (Instron) with support pins placed 36 mm apart. The cross-head was moved at a rate of 10 mm/min. Maximum flexural strength was calculated from the maximum load using the following equation:

$$\sigma = \frac{3FL}{bd^2}$$

where F is the load at the fracture point, L is the length of the support span, b is the width of the bar, and d is the thickness of the bar. The maximum flexural strength for the LUMI arm was also calculated from this equation using the arm's dimensions.

Capsule fabrication

Three dimensional models of the capsule pieces were created in Solidworks and printed on an Objet 30 Pro 3D printer. The two body portions of the capsule were adhered together by

spray coating Eudragit S100 onto the piece as they were clasped together. Eudragit spray coating was performed as per the published Evonic guidelines. Briefly, 342.9 g of acetone, 514.2 g of isopropanol, and 42.9 g of water were combined to create a diluent mixture. Then, 62.50 g of the Eudragit polymer was added to 50% of the diluent mixture and stirred for 60 minutes. At the same time, 6.25 g of triethyl citrate and 31.25 g of talc were added to the remaining diluent mixture and stirred for 10 minutes. The excipient suspension was then added to the Eudragit suspension, stirred for 5 minutes, and then passed through a 0.5 mm sieve. The combined solution was spray coated using a Master Economy E91 Single-Action airbrush set with a 0.8 mm tip and a 3.175 mm air inlet (TCPGlobal, San Diego, USA). The inlet stream was compressed nitrogen pressurized to 0.1 MPa. The spray coating process yielded a coating at least 20 μm thick. The capsule piece holding the spring was press fit into one portion of the capsule's body. A spring with a compressed length of 4.1 mm, a load of 1.3 N, and a free length of 31.8 mm (Spring CI 011EF 11S, Lee Spring, Brooklyn, USA) was then trimmed to a length of 30 mm and cut in half. Using thread (Sparkfun, Niwon, USA), one half of the springs were tied to one section of the capsule, and the other half were tied to the plunger. The two spring halves were then placed inside the capsule in series. Pressure was applied on the plunger to fully compress the spring. Melted PEG was then fed through that of the capsule to freeze the spring in place. Molecular weights of PEG between 3,000 and 35,000 were used. The change in dissolution time allowed the capsule to release the device at different time intervals. The relationship between PEG molecular weight and capsule actuation was tested in a bath of SIF heated to 37°C. Eudragit L-100 55 was then spray coated onto that section of the device to coat the PEG using the same method described previously. The LUMI device was then placed inside of the capsule and the cap was pressed fit onto the other side of the capsule.

Microneedle fabrication

Positive microneedle master molds with varying microneedle heights were obtained from Novo Nordisk Devices and were machined out of 304 stainless steel. Negative molds were then fabricated by pouring PDMS over the positive master molds and baking them at a temperature of 60°C for 24 hours. The molds used for the LUMI device created microneedles with a height of 1 mm and a base diameter of 0.4 mm. Microneedles with heights varying from 600 μm – 1200 μm were also fabricated and tested for their ability to penetrate swine small intestine tissue (Fig. S11), but they were not used with the LUMI device.

Microneedle patches were fabricated with insulin concentrated in the tips. Solid insulin powder was placed in PDMS female microneedle molds and forced into the microneedle tips using a spatula. Excess powder was then removed from the mold. The amount of powder added to the mold was calculated by weighing the mold before and after the addition of powder. The accuracy of weight measurements was confirmed using high performance liquid chromatography. Briefly, we employed a 7.8 × 300 mm^2 insulin HMWP column (Waters Cerp, Milford, USA) set to room temperature and an Agilent (Santa Clara, USA) High Performance Liquid Chromatography (HPLC) machine. Elution were performed at a flow rate of 0.5 mL/min for 26 minutes using a mobile phase made from 15% acetic acid (v/v), 20% acetonitrile (v/v), and 0.65 g/L L-arginine all purchased from Sigma Aldrich. The

molds were then centrifuged at 3200 rcf for 10 minutes to compress the powder. Next, a 50% 58,000 molecular weight polyvinylpyrrolidone solution in deionized water or 100% sorbitol was added to bind the powder and give mechanical structure to the microneedle patches. The mold was then centrifuged again at 3200 rcf for 10 minutes. The microneedle patches were left to dry at room temperature for 72 hours. Once dried, microneedles patches were unmolded, sanded down and mounted onto the recessed edges of the LUMI arms. We loaded 0.3 mg of insulin per LUMI. The amount of API could be increased by further compressing the powder into the microneedles. A maximum insulin load of 0.5 mg per LUMI could be achieved.

The microneedles made from lysozyme and α-glucosidase were fabricated in the same manner. The amount of protein in the tips of these microneedle patches was determined via a bicinchoninic acid assay. The activity of lysozyme either in the microneedle formulation or as a lyophilized powder was performed by measuring the cell lysis of *Micrococcus lysodeikitcus* as per the Sigma Aldrich published protocol. The activity of α-glucosidase either in the microneedle formulation or as a lyophilized powder was performed using an activity assay kit that measured the hydrolysis of *p*-nitrophenyl-α-D-glucopyranoside. The activity of the proteins (Units/mg) in the patches were then compared to the activity of the unformulated, lyophilized proteins to determine their stability in the formulations.

Microneedle dissolution

Microneedle dissolution patterns and, in turn, drug delivery kinetics were studied using both insulin and Texas red-based fluorescent dyes. Microneedles loaded with Texas red and Texas red conjugated with dextran (3 kDa) were used to perform dissolution tests *in vivo* in swine prior to euthanasia and *ex vivo* in human small intestinal tissue. Microneedles were manually inserted for 5 s, 15 s and 30 s and then retrieved. A microneedle patch (0.30 g) was left to sit on top of the tissue without applying any external pressure for 30 s which served as the negative control. An in vivo imaging system (Perkin Elmer, Waltham, USA) was then used to assess the Texas red and Texas red-dextran transfer onto the tissue via fluorescence. Living Image® software (Perkin Elmer, Waltham, USA) was used to quantify the radiant efficiency. The same dissolution kinetics occurred when measuring dye transfer from microneedle patches to both *ex vivo* human and *in vivo* swine tissue (Figure 3d, 3f, S10). Over a 30 second time period, the inserted microneedles transferred twice as much dye to the tissue and six times as much insulin to the gel on average compared to the negative control.

The same dissolution test was performed using insulin microneedles in a 0.3% agarose gel. Insulin transferred to the gel was retrieved by chopping the hydrogel to facilitate insulin dissolution into 2 mL of a pH 3 phosphate buffer solution. Insulin was then quantified via HPLC. Up through 30 seconds, increasing contact time correlated with increasing levels of insulin transfer to a 0.3% agarose gel (Figure S9). This dissolution experiment was also performed *in vivo* with insulin-loaded microneedles. The microneedles were imaged using an optical microscope before and after their application in the small intestine tissue to visually assess their dissolution.

Microneedle penetration

A 1.3 μm wavelength optical coherence tomography (OCT) system developed at MIT and optical microscopy were used to visualize penetration of the microneedles into excised small intestine from swine (Figure 3i, S11-S13). For this, various microneedle arrays were inserted *ex vivo* into the tissue via manual application and OCT was used to evaluate both penetration depth and dissolution. In addition, a fixture (Figure S15) was designed in order to hold the LUMI and deploy one of its arms in a 30° angle into a certain point of an *ex vivo* swine small intestine piece in order to promptly capture the penetration event prior to microneedle dissolution. In this latter case, the OCT image was captured from the outside of the tissue wall instead of from behind the patch, allowing the assessment of perforation. OCT images were processed using Image J (Open Source).

Penetration of the microneedles attached to the LUMI into small intestine tissue was also tested by performing histology and microCT on *ex vivo* swine tissue. MicroCT imaging was performed on a GE CT120 microCT imaging system (General Electric, Boston, USA). The devices were deployed with either sharpened metal hypodermic needles or with microneedles loaded with barium sulfate (Sigma Aldrich). The needles were also coated in a tissue marking dye (Cancer Diagnostics Inc, Durhan, USA) in order to mark the area of tissue penetration for histology.

In vivo testing and pharmacokinetic modeling

All animal experiments were approved by and performed in accordance with the Committee on Animal Care at MIT. To assess the insulin microneedle formulation, we administered the API formulation to female Yorkshire swine, 35 kg to 65 kg. To deliver the LUMI devices, we placed the swine on a liquid diet for 24 hours before the procedure and fasted the swine overnight. We then sedated them with an intramuscular injection of Telazol (tiletamine/zolazepam) (5 mg/kg), xylazine (2 mg/kg), and atropine (0.05 mg/kg) along with supplemental isoflurane (1 – 3% in oxygen) via a face mask. An orogastric tube or overtube was placed with guidance of a gastric endoscope and remained in the esophagus to ease the passage of the device. The overtube was passed through the stomach and into the small intestine. Encapsulated LUMI devices were passed through the overtube and placed into the small intestine. Non-encapsulated LUMI devices were inserted and actuated during a non-survival procedure whereby a ventral midline laparotomy was performed to access the small intestine. A 3 cm incision was made in the intestinal wall to access the mucosa. During these non-survival experiments, the size of the small intestine was standardized to 20 mm in diameter by applying a clamp to the tissue. The microneedles delivered manually to the small intestine were also inserted during a similar laparotomy procedure in which a 3 cm incision was used to access the small intestinal mucosa, and a microneedle patch was manually inserted into the intestinal surface epithelium. Patches with an area of 1 cm^2 were applied to the jejunum of the swine. Pressure was applied to the patch for 30 s, and then the patch was removed from the small intestine. To create the subcutaneous dose required for administration the microneedles from four patches were dissolved into 2 mL of sterile saline (Hospira, Lake Forest, USA). The mixture was then filtered through an Acrodisc 0.2 μm low protein binding filter (Pall Life Sciences, Westborough, USA) and 0.5 mL of the resulting solution was administered to each swine subcutaneously. Lastly, the insulin solution dosed to

the jejunum was prepared by dissolving the microneedles from one patch into 10 mL of water purified using a Barnstead Nanopure system (ThermoFisher, Waltham, USA). The solution was then passed through an endoscope directly into the jejunum of the swine.

We obtained blood samples via a central venous line at time points including but not limited to every 10 minutes for the first two hours and every 30 minutes for hours 2–4. We immediately tested blood samples for glucose levels using a OneTouch Ultra glucose monitor by LifeScan Inc. (Milpitas, USA). We collected additional blood into Ethylenediaminetetraacetic K3 tubes (Sarstedt, Numbrecht, Germany) and spun them down at 2000 rcf for 15 minutes. Collected plasma from MIT was shipped on dry ice to Novo Nordisk in Maalov, Denmark, and blood was analyzed there via an AlphaLisa developed at Novo Nordisk. Briefly, the homogenous bead assay employed two monoclonal antibodies against human insulin, creating an acceptor-bead, insulin, and donor-bead layering. This generated a signal which was proportional to the concentration of insulin. Additionally, blood was analyzed at MIT using an ELISA developed at Novo Nordisk. Both tests utilized antibodies specific for human insulin and neither test detected other endogenous insulins.

The data extrapolation performed on the *in vivo* plasma insulin data was performed by first isolating the data points from the small intestine patch and the subcutaneous dose after the t_{max}. The log of the concentration values was then plotted on the y axis over time, and a linear trend line was fit to the data. In order to estimate the area under the curve after the sampled time points, the slope of the trend line was multiplied by 2.303 and the resulting value was divided into the final plasma insulin concentration measured *in vivo*. The resulting number was an estimate for the area under the curve expected from the plasma insulin concentration curve after the final time point was taken. This value was added to the area under the curve calculated from the concentration values determined from the *in vivo* blood sampling to estimate the total area under the curve from a given dose.

Specialized LUMI devices were administered to the swine to determine the capsule actuation time as well as the transit and dissolution timeline for the LUMI. These LUMI devices contained small pieces of metal material such as nitinol or stainless steel which allowed the device to be seen when radiographed. The swine were radiographed over several hours in the case of the capsule actuation experiments. The swine were radiographed over several days in the case of the transit experiments until the all of the metal components passed through the GI tract.

When taking histology, the animal was sacrificed 5–15 minutes after the delivery events so that an entire cross section of tissue could be examined at the exact point of device deployment. Tissue marking dye was used to denote the appropriate area for histology. Redness and bleeding were observed at the tissue sites of microneedle insertion immediately after the LUMI deployment and the direct insertion of microneedles, signifying tissue penetration. These phenomena rapidly disappeared within minutes, as confirmed via visual inspection of the tissue.

Supplementary Text

LUMI opening geometric analysis

A geometric analysis of the unfolding event defined a minimum arm length required to provide tissue stretch from any possible orientation. We assumed the small intestine possessed a known diameter (d) and the tissue was not rigid. The LUMI device could open up in any orientation, including: axial; parallel; or anywhere in between. An analysis of all possible orientations showed that the tissue would stretch the least in the configuration where the planes perpendicular to the central axis containing an arm's point of contact were spaced furthest apart. In this orientation the LUMI opened inside the small intestine as shown in the parallel deployment picture in Figure 2d. Specifically, one of the arms is pointing exactly perpendicular to the small intestine's axis. When deployed in this orientation, the arms contacted the tissue over the greatest possible surface area. Because this orientation stretched the tissue the least, we concluded that if the LUMI stretched the tissue in this orientation then it would stretch the tissue in any other possible orientation.

During ex vivo and in vivo studies, we noticed that the small intestine conformed to the LUMI and changed shape. When the LUMI device unfolded in the parallel direction, the tissue transformed from a cylinder and collapsed into two parallel rectangular sheets. If the tissue did not stretch at all in the vertical direction due to the LUMI unfolding event, then each of these sheets would be of equal surface area. Because the surface area of the small intestine remained constant, the side length of this newly created rectangle sheet equaled ½ of the small intestine's perimeter ($\pi d/2$).

Next, we took into account the relationship between the LUMI arm length and the rectangular side length. Each LUMI arm is angularly positioned exactly 120° away from its neighboring arms. Therefore, we know that the height of the triangle created by the tips of each LUMI arm corresponds to 1.5 times the LUMI arm length. We also know that the LUMI unfolding position which creates the least amount of stretch in the small intestine occurs when the LUMI opens in a position where the height of the triangle is in the same direction as the side length of the rectangular sheet created by the tissue. In order to ensure that the tissue stretched, the LUMI triangle height needed to exceed the rectangle side length. Therefore, we determined that the arm length needed to exceed $\pi d/3$ in order to force the small intestine to stretch when the LUMI opened.

Optimizing the arm force on the tissue:

Varying the arm length and unfolding angle affected the amount of force delivered by the LUMI arm (Figure 2f, 2k, S1). Devices with longer arms required less angular expansion before making contact with tissue compared to devices with shorter arms. The core, consisting of 76 μm thick spring steel shim stock embedded in Mediprene elastomer, delivered a greater amount of force at more acute unfolding angles.

The addition of the steel piece also increased the contact force between the arm and the impact point. This effect was not seen if the Mediprene material continued along the arm past the steel section. For example, in a 15 mm long Mediprene core with a 7 mm long steel section, there existed no significant change in contact force between a device with and

without the steel part (Figure 2f). In an 8 mm long core, adding the 7 mm long, 76 μm thick steel resulted in a 60% increase in contact force. Adding the steel piece also increased the force exerted for a 45° deflection and 180° torsion by 150% and 50% respectively (Figure 2g-h). Steel pieces thinner than 0.076 mm commonly broke after multiple tests and those thicker commonly ruptured the Mediprene coating.

In vivo, we tested the ability for LUMI devices with different arm lengths and cores to stretch the tissue. Devices oriented in all directions provided at least some tissue stretch, but axially oriented devices provided more stretch than parallel oriented devices. We noted that devices with 25 mm long arms oriented in the axial direction after opening more frequently than devices with 23 mm long arms (Figure 2i). We also noted that devices with 25 mm long arms containing a metal core oriented axially more frequently than ones without a metal core. Axially oriented devices stretched the tissue to a diameter of 40 mm at the tissue's narrowest point in the plane perpendicular to the tissue's central axis. Devices containing metal cores provided a greater tissue stretch than devices with cores that did not include metal when orienting in the parallel direction. These devices stretched the tissue to 12 and 10 mm, respectively (Figure 2j). Adding metal to the core also increased the likelihood of axial deployments because the increased force required for deflection limited the device's flexibility to change conformations.

Capsule Deployment

The capsule was designed to actuate after leaving the stomach and entering the duodenum. A Eudragit L-100/55 (Poly[methacylic acid-co-ethyl acrylate]) coating designed to dissolve at a pH of 5.5 or greater dissolved after being in the environment of the small intestine and exposed two holes on one end of the capsule. Exposing the holes allowed fluid to access the inside of the capsule's spring chamber. This fluid then started to dissolve a polyethylene glycol (PEG) coating encasing two compressed springs in series. Once dissolved, the springs propelled the LUMI device out of the capsule by pushing on a plunger inside of the capsule (Figure 2a). In their expanded state, each spring measured 15 mm in length or less. The ends of the springs were capped with a polycaprolactone coating to prevent them from perforating the intestinal wall. One spring was tied to the base of the capsule using SparkFun conductive thread (SparkFun, Boulder, USA) so that it would remain inside of the capsule walls as it passed through the GI tract. The other spring was tied to the plunger via two holes placed on the bottom of the plunger using the same conductive thread. After the LUMI device was released, it unfolded and delivered the microneedle patches to the intestinal wall. The elastomeric core of the LUMI exited the capsule last, protecting the microneedles from shearing or compressing against the capsule structure.

LUMI fabrication for potential high throughput production:

LUMI fabrication began with the core which was milled to shape. In a scaled-up process, the metal core could be stamped using a steel die. The next step was encapsulating the core with an elastomer. In order to fabricate proof of concept LUMI cores, we casted two halves of the elastomeric core, then we placed the metal core between each half and re-melted the cores together. This casting and re-melting process could be replaced with an over-mold injection molding process around the steel core. In the lab setting, the LUMI arms were fabricated by

microcompounding together Soluplus® and PEG and casting the mixture to shape. The microcompounding could be scaled up, and the casting could be replaced with injection molding. Each of the injection molding steps could be executed in series in an assembly line, and overmolding techniques could be used to join each component. The LUMI microneedles were solvent casted. This process is being scaled up commercially for the purpose of transdermal drug delivery, and a similar process would be used during scaled-up LUMI manufacturing. The microneedles could be attached to the LUMI arms using a snap fit, press fit, or other locking mechanism during the scaled-up process.

During our proof of concept study, the capsule pieces were 3D printed, but these pieces could be injection molded in a commercial setting. Assembly of the capsule pieces could be performed using one of the locking mechanisms described above. The spring and the LUMI device could be placed inside of the capsule during the assembly process. Fixing the compressed spring was performed in the study by casting the spring inside of the capsule, and during scale up this process could be performed using injection molding to cast the spring. Coating the capsule in an enteric polymer was performed using a spray coat process, and this process could be scaled up in a commercial setting.

Supplementary Material

Refer to Web version on PubMed Central for supplementary material.

Acknowledgements:

We thank S. McDonnell, K. Ishida, J. Haupt and M. Jamiel for help with the *in vivo* porcine work. We thank Christoph Steiger and Yong Lin Kong for their helpful conversations on the capsule system. We thank J. Bales and the Edgerton Center at MIT for providing a high-speed camera setup. We thank Ania Hupalowska for her illustrations of the LUMI concept. We thank the Koch Institute for Integrative Cancer Research at MIT's histology core. We thank the National Disease Research Interchange for their help with the procurement of human tissue. We would like to thank Uli Stilz, Mia Bielecki, Thomas Kjeldsen, Lars Fogh Iversen, Jacqueline Trosborg, Peter Herskind, Rikke Kaae Kirk, Morten Revsgaard Frederiksen, František Hubálek, Jorrit J. Water, Anders V. Friderichsen, Stephen Buckley, Andreas Vegge, and Tina Bjeldskov Pedersen for helpful discussions throughout the development of the LUMI. We are grateful to Raissa Yona and all other members of the Langer and Traverso laboratories and Novo Nordisk for their expertise and discussions around biologic drug delivery.

Funding: This work was funded in part by a grant from Novo Nordisk, NIH Grant No. EB-00244. A.A. was supported in part by the NSF GRFP fellowship. G.T. was supported in part by the Division of Gastroenterology, Brigham and Woman's Hospital and the Department of Mechanical Engineering, MIT. M.K., D.D., D.S. were supported by the MIT Undergraduate Research Opportunities Program (UROP) program. N.R. was supported in part by the Olof Viking Bjork scholarship trust. H.L., T.Y. and J.F. were supported in part by NIH R01-CA075289–21.

References:

1. Korytkowski M When oral agents fail: practical barriers to starting insulin. Int. J. Obes 26, S18–S24 (2002).
2. Inzucchi SE et al. Management of hyperglycemia in type 2 diabetes, 2015: a patient-centered approach: update to a position statement of the American Diabetes Association and the European Association for the Study of Diabetes. Diabetes Care 38, 140–9 (2015). [PubMed: 25538310]
3. Matza LS et al. Utilities and disutilities for type 2 diabetes treatment-related attributes. Qual. Life Res 16, 1251–1265 (2007). [PubMed: 17638121]
4. Boye KS et al. Utilities and disutilities for attributes of injectable treatments for type 2 diabetes. Eur. J. Heal. Econ 12, 219–230 (2011).

5. Abramson A et al. An ingestible self-orienting system for oral delivery of macromolecules. Science (80-.) 363, 611–615 (2019).
6. Dallel N, Kacem M, Nabouli RM & El May M [Disposal of insulin syringes by diabetic patients. Report of 100 patients]. Tunis. Med 83, 390–2 (2005). [PubMed: 16220694]
7. Turner RC, Cull CA, Frighi V, Holman RR & Group, for the U. P. D. S. (UKPDS). Glycemic Control With Diet, Sulfonylurea, Metformin, or Insulin in Patients With Type 2 Diabetes Mellitus<SUBTITLE>Progressive Requirement for Multiple Therapies (UKPDS 49)</SUBTITLE> JAMA 281, 2005 (1999). [PubMed: 10359389]
8. Pratley RE et al. Liraglutide versus sitagliptin for patients with type 2 diabetes who did not have adequate glycaemic control with metformin: a 26-week, randomised, parallel-group, open-label trial. Lancet 375, 1447–1456 (2010). [PubMed: 20417856]
9. Calvert MJ, McManus RJ & Freemantle N Management of type 2 diabetes with multiple oral hypoglycaemic agents or insulin in primary care: retrospective cohort study. Br. J. Gen. Pract 57, (2007).
10. Holman RR et al. Addition of Biphasic, Prandial, or Basal Insulin to Oral Therapy in Type 2 Diabetes. N. Engl. J. Med 357, 1716–1730 (2007). [PubMed: 17890232]
11. Rubino A, McQuay LJ, Gough SC, Kvasz M & Tennis P Delayed initiation of subcutaneous insulin therapy after failure of oral glucose-lowering agents in patients with Type 2 diabetes: a population-based analysis in the UK. Diabet. Med 24, 1412–1418 (2007). [PubMed: 18042083]
12. Harrison GA Insulin in Alcoholic Solution by The Mouth. Br. Med. J 2, 1204–5 (1923). [PubMed: 20771392]
13. Derrickson BH & Tortora GJ Principles Of Anatomy And Physiology (Wiley, 2008).
14. Traverso G et al. Microneedles for Drug Delivery via the Gastrointestinal Tract HHS Public Access. J Pharm Sci 104, 362–367 (2015). [PubMed: 25250829]
15. Aguirre TAS et al. Current status of selected oral peptide technologies in advanced preclinical development and in clinical trials. Adv. Drug Deliv. Rev 106, 223–241 (2016). [PubMed: 26921819]
16. Caffarel-Salvador E, Abramson A, Langer R & Traverso G Oral delivery of biologics using drug-device combinations. Curr. Opin. Pharmacol 36, 8–13 (2017). [PubMed: 28779684]
17. Tibbitt MW, Dahlman JE & Langer R Emerging Frontiers in Drug Delivery. J. Am. Chem. Soc 138, 704–717 (2016). [PubMed: 26741786]
18. Vllasaliu D, Thanou M, Stolnik S & Fowler R Recent advances in oral delivery of biologics: nanomedicine and physical modes of delivery. Expert Opin. Drug Deliv 15, 759–770 (2018). [PubMed: 30033780]
19. Davies M et al. Effect of Oral Semaglutide Compared With Placebo and Subcutaneous Semaglutide on Glycemic Control in Patients With Type 2 Diabetes. JAMA 318, 1460 (2017). [PubMed: 29049653]
20. Banerjee A et al. Ionic liquids for oral insulin delivery. Proc. Natl. Acad. Sci. U. S. A 115, 7296–7301 (2018). [PubMed: 29941553]
21. Mathiowitz E et al. Biologically erodable microspheres as potential oral drug delivery systems. Nature 386, 410–414 (1997). [PubMed: 9121559]
22. Pridgen EM, Alexis F & Farokhzad OC Polymeric nanoparticle drug delivery technologies for oral delivery applications. Expert Opin. Drug Deliv 5247, 1–15 (2015).
23. Fox CB et al. Fabrication of Sealed Nanostraw Microdevices for Oral Drug Delivery. ACS Nano 10, 5873–5881 (2016). [PubMed: 27268699]
24. Banerjee A, Wong J, Gogoi R, Brown T & Mitragotri S Intestinal micropatches for oral insulin delivery. J. Drug Target 25, 608–615 (2017). [PubMed: 28266884]
25. Mitragotri S, Burke PA & Langer R Overcoming the challenges in administering biopharmaceuticals: formulation and delivery strategies. Nat. Rev. Drug Discov 13, 655–72 (2014). [PubMed: 25103255]
26. Vazharov IP Perforation as a complication of the diagnostic upper and lower endoscopy of the gastrointestinal tract. in Journal of IMAB -Annual Proceeding 18, (2012).

27. Eisen GM et al. Complications of upper GI endoscopy. Gastrointest. Endosc 55, 784–793 (2002). [PubMed: 12024128]
28. Webb WA Management of foreign bodies of the upper gastrointestinal tract: Update. Gastrointest. Endosc 41, 39–51 (1995). [PubMed: 7698623]
29. Velitchkov NG, Grigorov GI, Losanoff JE & Kjossev KT Ingested foreign bodies of the gastrointestinal tract: Retrospective analysis of 542 cases. World J. Surg 20, 1001–1005 (1996). [PubMed: 8798356]
30. Podolsky DK Healing the epithelium: Solving the problem from two sides. J Gastroenterol 32, 122–126 (1997). [PubMed: 9058308]
31. Wallace JL & Granger DN The cellular and molecular basis of gastric mucosal defense. FASEB 10, 731–40 (1996).
32. Fallingborg J Intraluminal pH of the human gastrointestinal tract. Dan. Med. Bull 46, 183–96 (1999). [PubMed: 10421978]
33. Coffey JW, Meliga SC, Corrie SR & Kendall MAF Dynamic application of microprojection arrays to skin induces circulating protein extravasation for enhanced biomarker capture and detection. Biomaterials 84, 130–143 (2016). [PubMed: 26826791]
34. Gatto NM et al. Risk of Perforation After Colonoscopy and Sigmoidoscopy: A Population-Based Study. JNCI J. Natl. Cancer Inst 95, 230–236 (2003). [PubMed: 12569145]
35. Bass DM, Prevo M & Waxman DS Gastrointestinal Safety of an Extended-Release, Nondeformable, Oral Dosage Form (OROS: A retrospective Study). Drug Saf 25, 1021–1033 (2002). [PubMed: 12408733]
36. Iddan G, Meron G, Glukhovsky A & Swain P Wireless capsule endoscopy. Nature 405, 417–417 (2000).
37. Sandler RS, Stewart WF, Liberman JN, Ricci JA & Zorich NL Abdominal Pain, Bloating, and Diarrheain the United States: Dig. Dis. Sci 45, 1166–1171 (2000). [PubMed: 10877233]
38. Camilleri M et al. Prevalence and Socioeconomic Impact of Upper Gastrointestinal Disorders in the United States: Results of the US Upper Gastrointestinal Study. Clin. Gastroenterol. Hepatol 3, 543–552 (2005). [PubMed: 15952096]
39. Hellmig S et al. Gastric emptying time of fluids and solids in healthy subjects determined by 13 C breath tests: influence of age, sex and body mass index. J. Gastroenterol. Hepatol 21, 1832–1838 (2006). [PubMed: 17074022]
40. Wang YR, Fisher RS & Parkman HP Gastroparesis-Related Hospitalizations in the United States: Trends, Characteristics, and Outcomes, 1995–2004. Am. J. Gastroenterol 103, 313–322 (2008). [PubMed: 18047541]
41. Cole ET et al. Enteric coated HPMC capsules designed to achieve intestinal targeting. Int. J. Pharm 231, 83–95 (2002). [PubMed: 11719017]
42. Kim YC, Park JH & Prausnitz MR Microneedles for drug and vaccine delivery. Adv. Drug Deliv. Rev 64, 1547–1568 (2012). [PubMed: 22575858]
43. Ye Y, Yu J, Wen D & Kahkoska AR Polymeric microneedles for transdermal protein delivery. Adv. Drug Deliv. Rev 127, 106–118 (2018). [PubMed: 29408182]
44. van Meer L et al. Injection site reactions after subcutaneous oligonucleotide therapy. Br. J. Clin. Pharmacol 82, 340–351 (2016). [PubMed: 27061947]

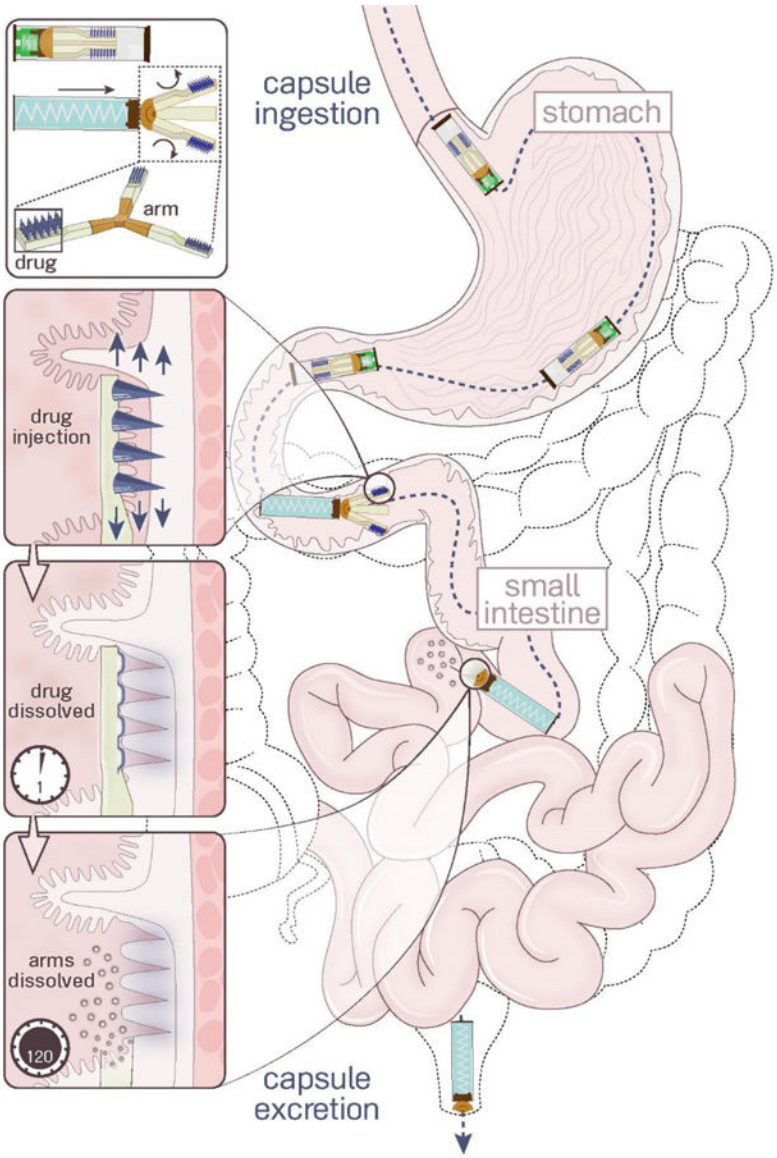

Fig. 1.

Luminal Unfolding Microneedle Injector (LUMI) design. LUMI devices were ingested in waterproof enteric capsules. They actuated and unfolded in the small intestine, injecting drug loaded microneedles into the tissue wall. The microneedle patches and arms dissolved within several hours. The non-degradable parts of the device passed through the GI tract and were excreted.

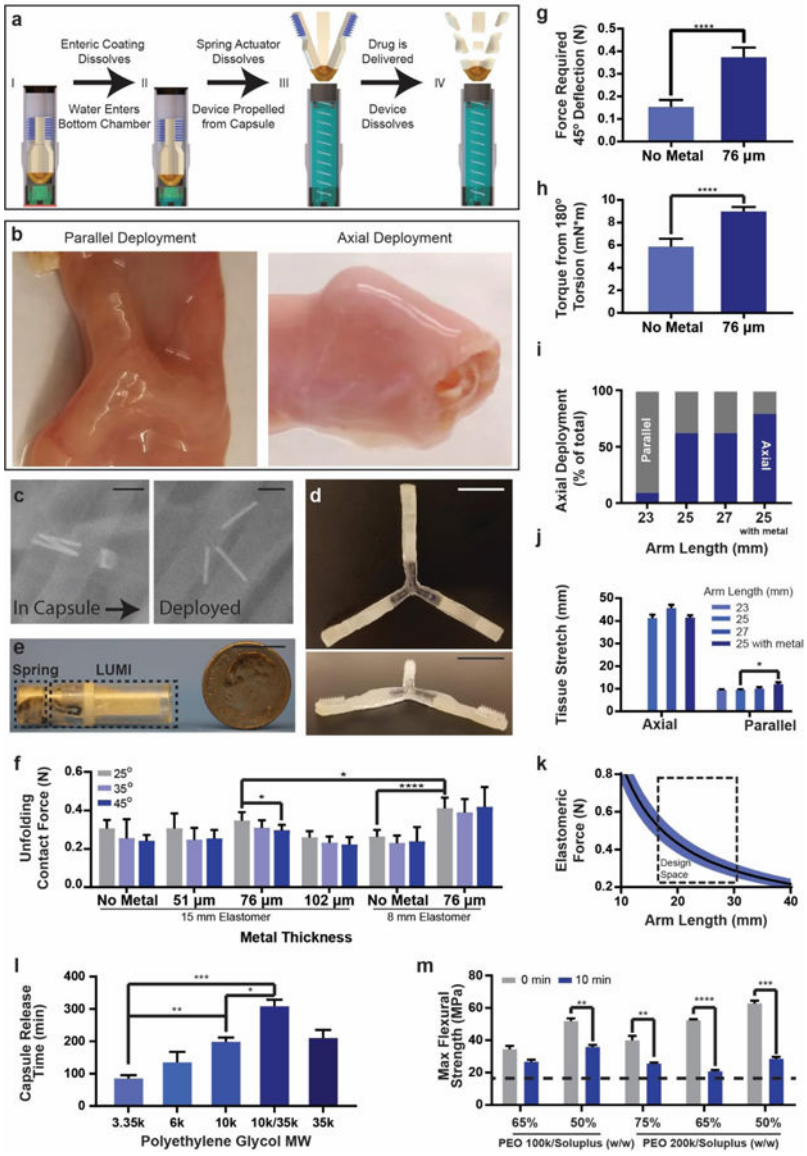

Fig. 2.

LUMI fabrication and design specifications. (a) The LUMI device was housed inside of a waterproof chamber until it reached the small intestine. After delivering the LUMI, the capsule broke apart into small pieces and passed through the GI tract. (b) LUMI devices opened up in multiple orientations in the small intestine, including in the parallel or axial directions shown in this figure. (c) X-rays confirmed that the capsule actuated and released the LUMI device within 2 hours. The metal rods were used for imaging purposes and were not part of the final design. (d) Photo of an unfolded and (e) encapsulated LUMI. (f) Unfolding contact force applied by the arm (n=9). (g) Forces required for arm deflection and (h) torsion (n=9). (i) Percent of devices deployed axially *in vivo* (n=15). (j) Tissue stretch from unfolding (n=9). (k) LUMI design space based on arm length and elastomeric force beneficial for administration. (l) Capsule Release time is dependent on molecular weight of PEG coating (n=3). (m) Arm flexural strength before and after dissolution in simulated

intestinal fluid at 37°C. The dotted line represented the calculated flexural stress required to break the LUMI arm (n=3). (Error Bars=SD; *P<0.05, **P<0.01, ***P<0.001, ****P<0.0001) Scale Bars are 1 cm.

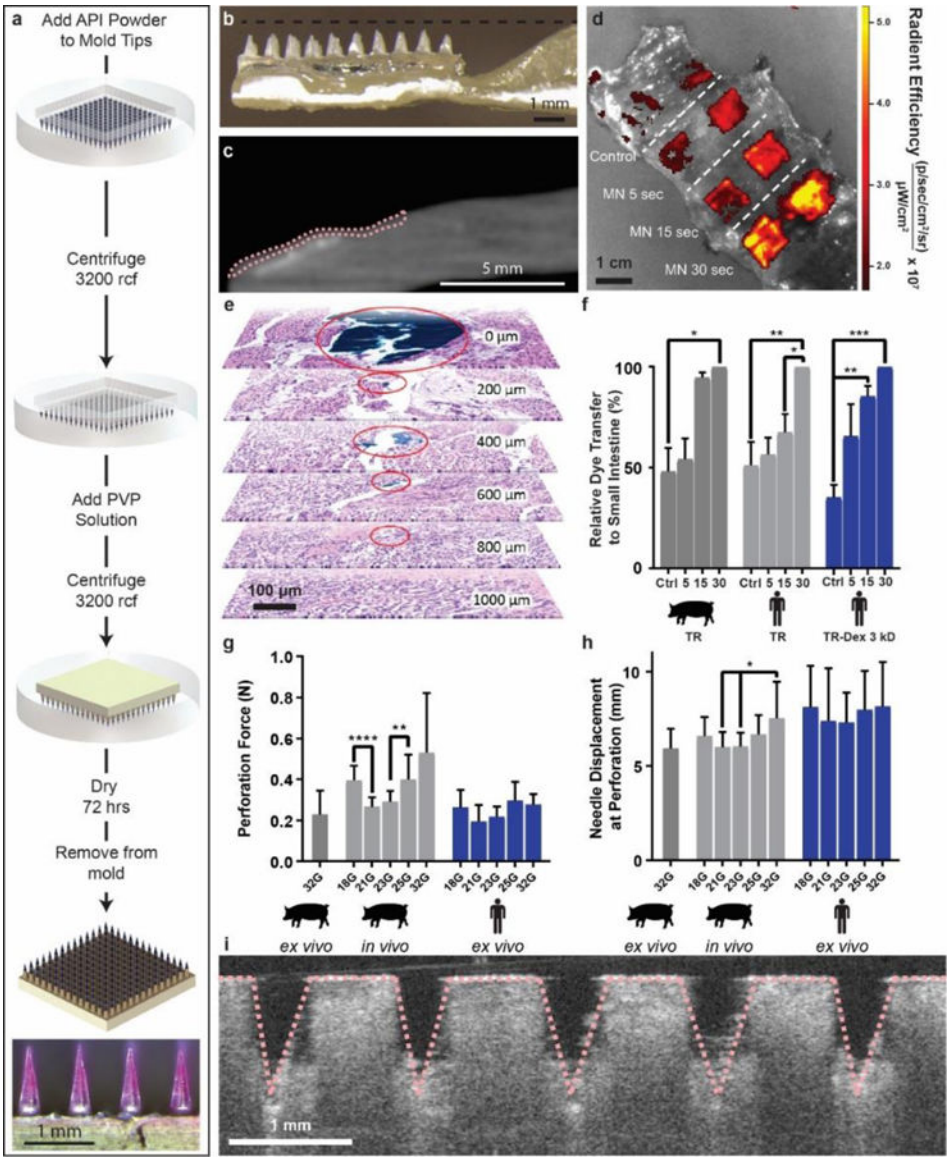

Fig. 3.

Polyvinylpyrrolidone microneedle (MN) characterization in the small intestine. (a) Microneedles were fabricated using solid API powder to increase their drug loading. A single patch 1 cm^2 held up to 0.6 mg in the tips alone. The microneedle patch pictured contained Texas red dye. (b) LUMI arms contained an indentation to house insulin loaded microneedles during encapsulation. (c) MicroCT image of a barium sulfate loaded microneedle patch applied to a section of human small intestine using the LUMI. The tissue is outlined in pink. (d) Texas red microneedle dissolution in human tissue. In the control experiment, patches were not penetrated into tissue but were left on the tissue for 30 s. (e) Histology confirmed that needles applied to the small intestine ex vivo using the LUMI penetrated but did not perforate the tissue. Surgical dye used to coat the needle reached 800 µm below the surface of the tissue (f) Relative dye transfer over time (seconds) of microneedles to small intestine tissue (n=3 over 3 samples). (g) Force and (h) displacement

required for needle perforation in the small intestine (n=15 over 3 samples). (i) Optical Coherence Tomography imaging confirmed that microneedles penetrated into the small intestine tissue. (Error Bars=SD; *P<0.05, **P<0.01, ***P<0.001, ****P<0.0001).

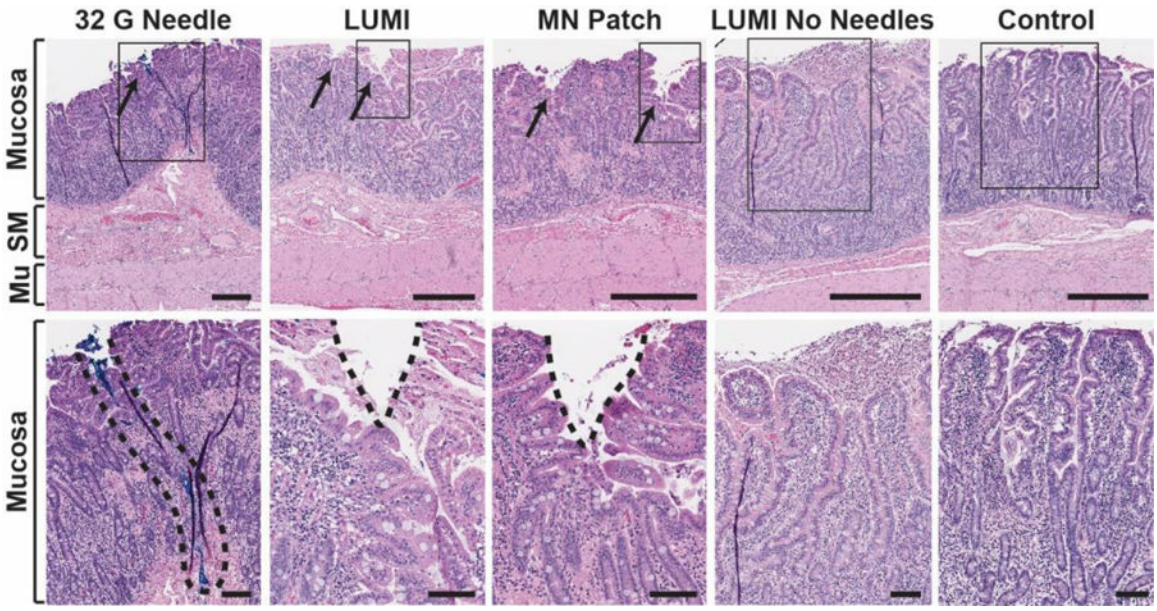

Fig 4.

In vivo histology. Hematoxylin and eosin stained swine small intestine tissue taken at the site of actuation. The top row represents a full tissue slice and the bottom row shows a zoomed in portion marked by the rectangular outline. From left to right: a 32 G hypodermic needle coated in blue dye was manually inserted into the tissue (dye is a surrogate for needle insertion depth, as no hole in the tissue was seen); a LUMI with microneedles unfolded and made contact with the tissue; a microneedle patch was manually applied to the tissue; a LUMI without microneedles unfolded and made contact with the tissue; a control piece of tissue where no device was applied. SM = Submucosa. Mu = Muscularis Externa. Scale Bars = 0.5 mm (top) 0.1 mm (bottom).

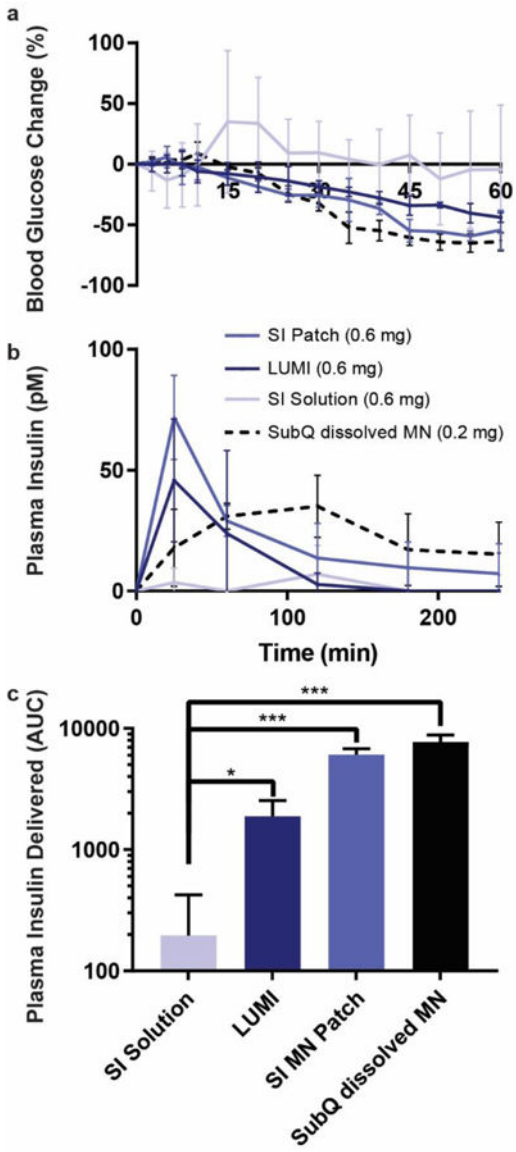

Fig 5.

In vivo insulin delivery via LUMI in swine. (a) Blood glucose and (b) plasma insulin levels are determined. Two LUMI devices were deployed in each swine jejunum and delivered a total of 0.6 mg of insulin in polyvinylpyrrolidone microneedle patches. Delivery was compared to an equivalent insulin dose from a microneedle patch dissolved in 10 mL water delivered to the lumen of the jejunum (SI Solution), a microneedle patch applied directly to the jejunum (SI MN Patch), or a microneedle patch dissolved in 0.5 mL of sterile saline, filtered and subcutaneously injected (SubQ dissolved MN) (n=3). After filtration some insulin was lost, and the subcutaneous insulin dose was calculated to be 0.2 mg. (c) The total plasma insulin (calculated using the area under the curve, AUC) delivered by each method after extrapolating the data out to infinite time. (Error Bars=SD; *P<0.05, ***P<0.001).